Inelastic neutron scattering evidence for anomalous H–H distances in metal hydrides

Andreas Borgschulte[a,b,1], Jasmin Terreni[a,b], Emanuel Billeter[a,b], Luke Daemen[c], Yongqiang Cheng[c], Anup Pandey[c], Zbigniew Łodziana[d], Russell J. Hemley[e,f,1], and Anibal J. Ramirez-Cuesta[c]

[a]Swiss Federal Laboratories for Materials Science and Technology (Empa), Laboratory for Advanced Analytical Technologies, CH-8600 Dübendorf, Switzerland; [b]Department of Chemistry, University of Zürich, CH-8057 Zürich, Switzerland; [c]Spallation Neutron Source, Neutron Spectroscopy Division, Oak Ridge National Laboratory, Oak Ridge, TN 37831-6475; [d]Institute of Nuclear Physics, Polish Academy of Sciences, PL-31342 Krakow, Poland; [e]Department of Physics, University of Illinois at Chicago, Chicago, IL 60607; and [f]Department of Chemistry, University of Illinois at Chicago, Chicago, IL 60607

Contributed by Russell J. Hemley, December 6, 2019 (sent for review July 26, 2019; reviewed by Malcolm Guthrie and Jinlong Zhu)

Hydrogen-containing materials are of fundamental as well as technological interest. An outstanding question for both is the amount of hydrogen that can be incorporated in such materials, because that determines dramatically their physical properties such as electronic and crystalline structure. The number of hydrogen atoms in a metal is controlled by the interaction of hydrogens with the metal and by the hydrogen–hydrogen interactions. It is well established that the minimal possible hydrogen–hydrogen distances in conventional metal hydrides are around 2.1 Å under ambient conditions, although closer H–H distances are possible for materials under high pressure. We present inelastic neutron scattering measurements on hydrogen in ZrV_2H_x showing nonexpected scattering at low-energy transfer. The analysis of the spectra reveals that these spectral features in part originate from hydrogen vibrations confined by neighboring hydrogen at distances as short as 1.6 Å. These distances are much smaller than those found in related hydrides, thereby violating the so-called Switendick criterion. The results have implications for the design and creation of hydrides with additional properties and applications.

intermetallic hydrides | hydrogen correlation | Switendick criterion | inelastic neutron scattering | diffusion

Quasi-free atoms in a rigid lattice have attracted great fundamental and technological interest. Archetypical examples are light elements such as hydrogen dissolved in metals (1) and Li intercalated in graphite (2). Some hydrogen–metal systems have great potential as hydrogen storage materials as hydrogen can enter and be released from the material because of its high diffusion coefficient (3). Also of interest are the high-temperature hydride superconductors, which were originally suggested (4) and found at megabar pressures, for example in LaH_{10} (5–7). Very high pressures can be used to increase the hydrogen content in known hydrides, as the maximum hydrogen content in intermetallic nonstoichiometric hydrides (berthollides) at modest pressure is much below the number of interstitial sites in the lattice that are accessible by hydrogen (8, 9). For this case, repulsive interactions, which increase at high hydrogen loading, diminish hydrogen capacity. One type of repulsive interaction is caused by electronic metal–hydrogen interaction in transition metals with almost completely filled d orbitals such as Pd (10, 11). The argument does not hold for early d-period elements (e.g., Ti, V, Zr, Hf). For these systems, local repulsive H–H interactions impede the occupation of neighboring sites with distances below 2.1 Å [so-called Switendick criterion (12, 13)], even if the attractive forces between hydrogen and metal atoms exist.

The Switendick limit is a consequence of the interaction between two protons and associated electrons. In molecular hydrogen with its H–H distance of 0.74 Å, the strongly repulsive Coulomb force of the protons is outweighed by the strong covalent interaction. In metal hydrides, a locally increased electron density between H atoms is reduced as the electrons from the hydrogen are distributed among other bonds in the material. As a result, the minimal possible hydrogen–hydrogen distance in conventional metal hydrides is around 2.1 Å under ambient conditions (13). To date, only one system violating the Switendick criterion has been found, i.e., in the rare earth (RE)-bearing compound, $RE_3Ni_3In_3D_{4\pm x}$, where the D–D distances are below 1.6 Å (14).

If a hydrogen atom occupies an interstitial site in a hydride lattice having crystallographically identical sites with distances below the Switendick limit, the occupation of that site precludes the occupation of neighboring interstices by other hydrogens. This is the case for ZrV_2. Experimentally, ZrV_2 absorbs up to approximately 6 [H]/[ZrV_2] (16), although uptake of 17 hydrogen atoms is possible if all tetrahedral interstices are occupied (17). At full occupancy, some distances between nearest-neighbor hydrogen interstices would be as short as 1.6 Å (18), which would fall well below the Switendick limit (Fig. 1). Thus, the distribution of hydrogen atoms in ZrV_2 is not expected to be random but a result of the optimization of short-range correlations that avoid direct next-neighbor interactions (18). Although there are indications of such correlations (18),

Significance

Hydrogen in metals alters the electronic structure of such materials and hence modifies the physical and chemical properties. In conventional transition metal hydrides containing atomic hydrogen, the minimum hydrogen–hydrogen distances are around 2.1 Å under ambient conditions (Switendick criterion). Although hints of H–H distances below 2.1 Å in AB_2 alloys have been reported, evidence is inconclusive as hydrogen positions are difficult to locate by diffraction techniques. Here, inelastic neutron scattering is used as a local probe of the hydrogen interactions together with electronic structure modeling of a well-studied and prototypical metal hydride ZrV_2H_x. The results provide evidence for anomalous hydrogen–hydrogen distances as short as 1.6 Å. The findings provide insights leading to the creation of materials with properties such as very high T_c superconductivity and other quantum behaviors.

Author contributions: A.B., J.T., L.D., Y.C., A.P., Z.Ł., and A.J.R.-C. performed research; A.B., J.T., E.B., L.D., Y.C., A.P., Z.Ł., and A.J.R.-C. analyzed data; A.B. and A.J.R.-C. found the anomaly; and A.B., J.T., E.B., R.J.H., and A.J.R.-C. wrote the paper.

Reviewers: M.G., European Spallation Source; and J.Z., Southern University of Science and Technology.

The authors declare no competing interest.

[1]To whom correspondence may be addressed. Email: rhemley@uic.edu or andreas.borgschulte@empa.ch.

This article contains supporting information online at https://www.pnas.org/lookup/suppl/doi:10.1073/pnas.1912900117/-/DCSupplemental.

First published February 6, 2020.

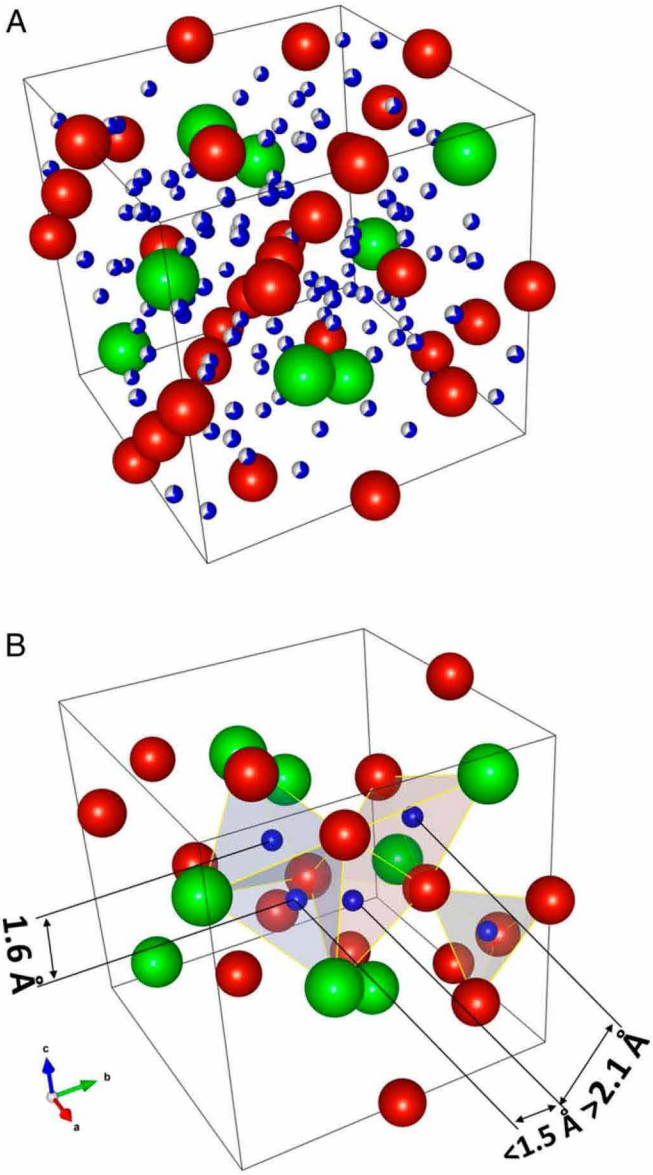

Fig. 1. Visualization of the crystal structure of ZrV_2H_4 (space group Fd3m). Green, red, and blue balls are zirconium, vanadium, and hydrogen atoms, respectively, based on the structure parameters from ref. 15 with $a =$ 7.8704(1) Å. *A* shows all 96*g* and 32*e* sites possibly occupied by hydrogen. The color filling indicates the partial occupation. *B* emphasizes the hydrogen coordination in the lattice. The hydrogen 32*e* sites are coordinated by three vanadium atoms and one zirconium (denoted as ^{T}H in the text). The 96*g* sites are coordinated with two vanadium and two zirconium atoms (denoted as ^{O}H). The gray tetrahedron is for unstable 8*a* site with four V neighbors. To simplify the visualization only few tetrahedrons are shown. For nearest 96*g* sites the corresponding H–H distance violates the Switendick criterion (1.5 to 1.6 Å, blueish tetrahedra facing each other). With this hydrogen content, only ~40% of all interstices are occupied, resulting in stochastic distribution. A representation of the crystal structure highlighting the hydrogen positions is given in *SI Appendix*, Fig. S1.

definitive evidence is missing, in part due to the limitations of existing experimental methods. Diffraction techniques probe the space- and time-averaged structure and give fractional occupancies (17) that hide the local H–H coordination. On the other hand, experimental techniques that give the average structure may be complemented by calculations of many possible configurations with different local structures corresponding to diffraction fractional occupation of sites. In this paper, we use such a combinatorial approach for the simple system ZrV_2 to support and interpret the experimental results.

Inelastic neutron scattering (INS) is a powerful technique to study the vibrational properties of materials and gives insights into the bonding and other properties (19). The method exploits the slightly different behavior between bound and free atoms during the scattering process and uses the difference in energy and momentum transfer to construct the phonon band structure of the system (19). The advantage of INS compared to the related Raman scattering (i.e., inelastic photon scattering) and infrared spectroscopies (infrared [IR] absorption and reflectivity) is its independence of optical selection rules (20). Moreover, phonons in metals cannot readily be detected by IR techniques (21), and Raman scattering from metals is weak due to the screening of electromagnetic radiation by quasi-free electrons (20). In contrast, neutrons do not interact with electrons and sample the entire Brillouin zone (different k vector and momentum transfer), while Raman and IR are restricted to the zone center (Γ-point). Thus, the full vibrational spectra of many metal hydrides have been exclusively derived from INS measurements (e.g., refs. 19 and 22).

In a simplified picture, hydrogen in an interstitial site feels a potential resulting from repulsive interactions and attractive interactions from the binding of hydrogen to the d states of the metal. The corresponding vibration energies are of the order of 100 meV (8). However, this picture neglects the repulsive interaction of neighboring hydrogens as described above, which lowers the overall binding energy of hydrogen as well as the associated vibrational frequencies. This effect on the vibrational spectrum is probed here by INS spectroscopy (see *Materials and Methods* for experimental details). To better understand and interpret the experimental results, we performed atomistic first-principles calculations of the properties of ZrV_2 with various hydrogen stoichiometries and coordinations. Comparison of the calculated and measured INS spectra allows us to assign the observed peaks to the corresponding phonon modes, an analysis that is more robust than comparing calculated partial hydrogen density of phonon states with those derived iteratively from measured INS spectra (23). Extensive combinatorial calculations of the energetics of 3,200 different structures of hydrogen-loaded ZrV_2 support the findings regarding the H–H distances in the material.

Results

Inelastic neutron scattering provides an amplitude-of-motion and neutron incoherent cross-section weighted phonon density of states (19). Scattering of neutrons with an energy transfer of several millielectronvolts typically arises from phonons. Given the much higher cross-section of hydrogen (80.26 barn) relative to that of vanadium (5.1 barn) and zirconium (0.02 barn), the spectra reflect the hydrogen partial phonon density of states of ZrV_2H_x (Fig. 2). Of primary importance are the spectral features below 200 meV, as higher energies are the overtones of the ground-state vibrations. The spectra are dominated by peaks around 150 meV, which can be described by hydrogen vibrating in a local harmonic potential well, a local picture that neglects the periodicity of the environment. In fact, due to the strong H–M interactions, the dispersion of the optical phonons of the hydride lattice is negligible (width of the peaks is around 10 meV) and is thus sufficiently described as a local potential. In ZrV_2, sites with different binding energies are occupied by hydrogens in succession (Fig. 1).

The principal measurements were carried out using the high-resolution INS spectrometer VISION at the Spallation Neutron Source (SNS), Oak Ridge National Laboratory (ORNL). The number and frequencies of high-energy peaks can be readily assigned within this localized model in agreement with earlier studies (*SI Appendix*, Fig. S2) which were restricted to

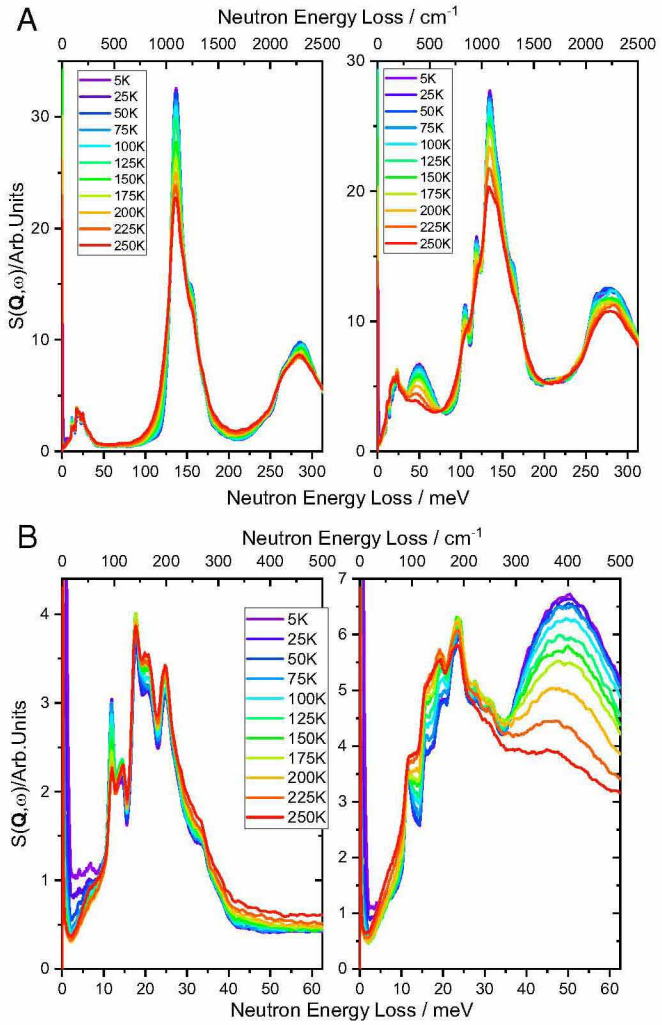

Fig. 2. Momentum-averaged inelastic neutron scattering at various temperatures as measured by the high-resolution neutron spectrometer VISION (*Materials and Methods*). (*A* and *B*) Full spectrum to 300 meV (*A*) and details of the low-energy range (*B*) of $ZrV_2H_{2.0}$ (*Left*) and $ZrV_2H_{3.7}$ (*Right*). In all cases, the intensity was corrected by the Bose–Einstein statistics to account for the temperature dependence of the scattering process. The color code indicating the measurement temperature is the same in all graphs.

measurements at high energies (24). The situation is different for acoustic phonons, which occur at low energies with the effective mass dominated by the metal atoms (25). Nevertheless, due to the dominant scattering of neutrons by hydrogen, the low-energy features present in the measurements can be assigned to hydrogen motions (sometimes called "riding modes"). Due to the high-energy resolution of the instrument, the fine structure of lattice vibrations around 20 meV is resolved (Fig. 2). Notably, for high hydrogen concentrations an additional peak is observed around 50 meV. The peak is located in a spectral region where no vibrations are expected, as a consequence of the difference in reduced mass and energy potentials of acoustic and optical phonons associated with the known hydrogen-binding energies in ZrV_2 (17). Vibrations at these low energies are usually assigned to acoustic phonons; however, the large width of the peak indicates that these excitations have a local character similar to the high-energy vibrations above 120 meV. Furthermore, the temperature behavior is the reverse of that observed and expected for acoustic phonons (*SI Appendix*, Figs. S4 and S5). The peak was experimentally confirmed in supplementary measurements performed at the MARI beamline at ISIS, United Kingdom (*SI Appendix*, Fig. S4).

Density functional theory (DFT) calculations were performed to understand the origin of the low-energy peak. The simulated INS spectra of ZrV_2H_2 match those measured experimentally, including both acoustic and optical phonon branches (Fig. 3). For the high-energy excitations, the calculated peaks are slightly higher in energy than the experimental data (e.g., 10 meV). We attribute this to the effects of anharmonicity (19), which also gives rise to the broadening of the high-energy peaks. On the other hand, the agreement breaks down for higher H concentrations. Most notably, no excitations in the spectral region around 50 meV are calculated by DFT if the hydrogen occupation of the interstices is constrained such that no H–H distances are less than 2.1 Å (Fig. 3). Also the splitting of the optical phonons is not well reproduced with this constraint.

Before assigning this peak to a new dynamic behavior of hydrogen, we considered possible alternatives such as the formation of chemisorbed hydrogen and desorption of hydrogen from ZrV_2 during cooling and subsequent condensation in liquid/solid form. Both cases do not reproduce the peak at 50 meV. Furthermore, the temperature dependence of the 50-meV peak demonstrates that the feature persists to temperatures as high as 250 K, which is well above the solidification and liquification temperature of hydrogen. Finally, we considered whether the peak is associated to hydrogen vibrations in pure vanadium. Under certain conditions (24), ZrV_2H_x can segregate into a Zr-rich alloy and VH_x phases. The dominant feature of INS of VH_x is around 55 meV (26) (*SI Appendix*, Figs. S2 and S4). This scenario cannot fully be excluded, as small amounts of V might indeed segregate that are not apparent by X-ray characterization (24). However, the total amount can be assumed to be small, while the observed peak is very prominent, which speaks against this explanation (for

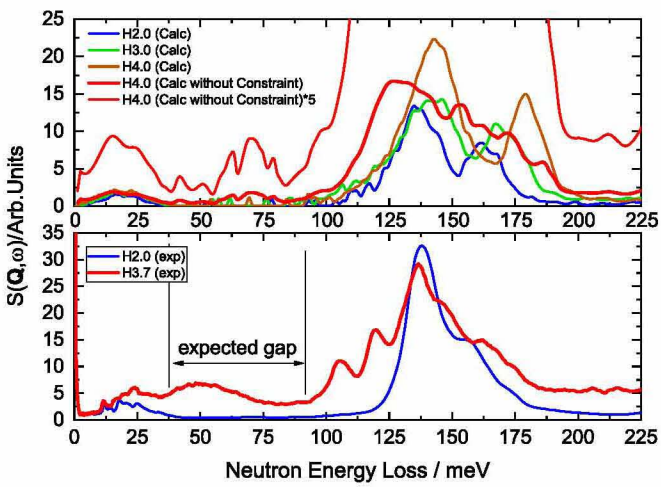

Fig. 3. Comparison of simulated INS (*Top*, blue, green, brown, and red curves, respectively) with experimental data measured at 5 K (*Bottom*, red and blue curves). Optical phonons (>100 meV $\simeq$ 750 cm^{-1}) are dominated by motion of hydrogens with a high amplitude and thus may be described as vibrations of hydrogen in a local potential. Vibrations below 50 meV are long-range lattice vibrations (acoustic phonons, riding modes), where hydrogens move with metal atoms. The expected gap between acoustic and optical phonons is observed at low hydrogen content and reproduced by DFT calculations omitting the occupation of interstices with H–H distances below 2.1 Å, irrespective of the hydrogen content. The peak arising in the gap needs the consideration of hydrogen violating the Switendick criterion as shown by the red curve. The simulation considering H–H distances below 2.1 Å has also a better agreement for the optical phonons at higher energies than the ones omitting short H–H distances (*SI Appendix*, Fig. S5).

further information we refer to *SI Appendix, Materials and Methods, Thermodynamic Properties of Zr-V-H*).

We performed additional extensive DFT calculations of ZrV_2H_4, taking into account various hydrogen configurations including those violating the Switendick criterion. Finite spectral intensity at around 50 meV occurs only when H–H distances are less than 2 Å (Fig. 3). The local structure with respect to hydrogens is given by the hydrogen pair density function $g_{H-H}(r)$ shown in Fig. 4. The number of hydrogen atoms violating the Switendick criterion is small, but sufficient enough to generate the unexpected peak at 50 meV and the splitting of the optical phonons (Fig. 3).

Additional information can be obtained from the calculated total energy of each hydrogen configuration (Fig. 5). From this we derive the most stable (i.e., lowest-energy) configuration and a measure of the binding energy of hydrogen in the lattice. As expected, the configuration without violating the Switendick criterion is the most stable one. On the other hand, the energy difference relative to the next higher configurations that include hydrogen with distances around 1.6 Å is of the order of only 0.5 eV/8 f.u. ($\simeq$ 1.5 kJ/[mol H]). That energy is easily overcome by entropic contributions at room temperature, where the hydrogen uptake takes place. As a multitude of configurations exist that can be populated, the violation of the Switendick criterion is therefore allowed under these thermodynamic conditions.

Discussion

In intermetallic hydrides, hydrogen can be viewed as a lattice gas with small covalent binding to the metal atoms (12). The potential well of hydrogen in the structure is thus less pronounced than in more complex hydrides, which results in easier hopping of hydrogen between sites (27). This facilitates diffusion of hydrogen in the material and forms the dominant contribution of the solution entropy to the total free energy of the system. An effect of this is that the maximum hydrogen capacity is usually smaller than the number of possible interstitial sites. In ZrV_2, various interstitial sites with different hydrogen-binding energies exist, as is typical in alloys and intermetallics. In a localized picture, the occupation of these sites starts with

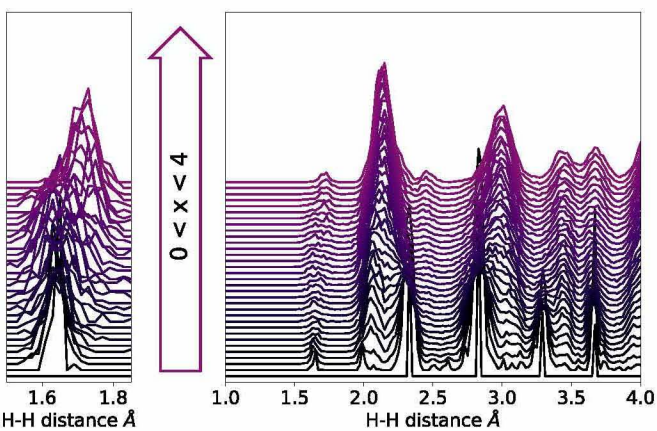

Fig. 4. Calculated pair density function of hydrogen atoms $g_{H-H}(r)$ in $ZrV_2\ {}^{T}H_{4-x}\ {}^{O}H_x$ without distance constraint as a function of the ${}^{O}H/{}^{T}H$ ratio, top $x = 4$, bottom $x = 0$ (for definition of sites compare Fig. 1). (*Left*) As the number of (^{O}H) sites increases a short H–H distance that violates the criteria appears around 1.6 Å. As the number increases, the center of the peak drifts to larger distances. (*Right*) The H–H distance from 1 to 4 Å. Note (*Right*) that there is is a peak above $\simeq$2.1 Å. The peak is centered at 2.0 Å only for $Zr_8V_{16}\ {}^{T}H_{31}\ {}^{O}H_1$; as the number of ^{O}H sites increases the peak shifts to values around 2.1 Å and above. On average the peak is centered at H–H > 2.1 Å.

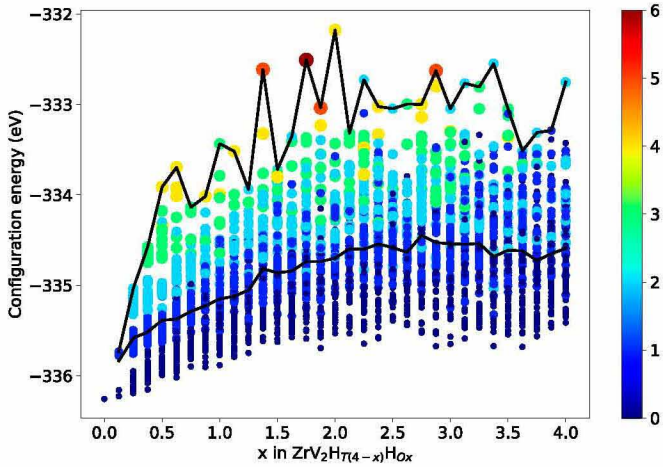

Fig. 5. Configurational energy per 8 formula units of ZrV_2H_4 with hydrogens occupying different sites. The color code visualizes the number of hydrogens with distances around 1.6 Å. If the (^{O}H) site is occupied ($x = 0$), Switendick's criterion will not be violated and is thus the most stable configuration. The number of violations increases to one with $x = 0.125$ and increases further as additional neighboring interstitials with H–H distances around 1.6 Å are found.

those having the highest binding energies, with the other sites occupied as the previous ones are completed. The corresponding pressure–composition isotherm has various distinct plateaus. The latter condition is softened in intermetallic hydrides with strong hydrogen–hydrogen interactions. In these cases, the maximum amount of hydrogen is not given by the availability of free interstitial sites, but by the hydrogen–hydrogen repulsion. Occupation of less stable sites occurs before completion of those that are more stable, which leads to a counterintuitive situation in which the occupation of sites with strong hydrogen–metal binding decreases with the increasing of the total hydrogen content in the solid (17). The resulting pressure–composition isotherm is a continuous increase of the equilibrium pressure with increasing hydrogen content (16), approaching Sieverts behavior for hydrogen in metals at low concentration.

We now discuss the implication of these findings for hydrogen in ZrV_2. Given the above, the configurational energy, and thus the total free energy, is practically a continuous function of the hydrogen site occupation (Fig. 5). The corresponding chemical potential of hydrogen in ZrV_2 is thus continuous as well. We refer to "hydrogen-binding energy" as the pure hydrogen–metal interaction, excluding the hydrogen–hydrogen interaction (compare also the definitions in refs. 10 and 11). The heat of formation per specific site, which includes both parameters, depends strongly on the occupancy (17). Atomic correlations are a key component of these dynamical phenomena, as the hopping of hydrogen in ZrV_2H_4 is assumed be correlated to satisfy the Switendick criterion of the minimum H–H separation (24). QENS measurements on ZrV_2H_x as well as the related material $Pr_2Fe_{17}H_5$ (28) confirm the existence of this correlated motion. As the diffusion of hydrogen in ZrV_2H_x is very fast compared to similar materials (24), the correlated motion does not appear to hinder hydrogen hopping, likely due to the possibility of violating the Switendick criterion.

An important question is whether the observed effect is limited to the specific compound ZrV_2. Measurements of hydrogen vibrations in 3d metal hydrides (22) do not show prominent features similar to the low-frequency peak. However, the hydrogen uptake is low in these hydrides, usually below one hydrogen per metal, and thus the H–H distances are well above the Switendick criterion. As mentioned in the Introduction, the limited hydrogen uptake in these metals is attributed to

electronic metal–hydrogen interactions that allow binding to a limited number of hydrogens per metal (29). This argument is not valid for elements in the beginning of the period. Structures similar to the low-energy peak have been found in AB_2 alloys containing vanadium (30) and in pure vanadium (26). In vanadium, interstitials with distances varying between 1.05 Å and 7.73 Å exist (12), but only the ones with minimum distances of 2.2 Å are observed by X-ray diffraction in V_2H (31). Calculations show that hydrogen–hydrogen interaction in vanadium becomes weakly attractive for distances between 2.1 and 2.5 Å (32), despite the hydrogen atoms avoiding occupying interstitial sites having short distances at or below the Switendick limit. The corresponding hydrogen pair has a calculated binding energy of 0.01 eV. As this binding energy is much smaller than the binding energy between V and H (0.32 eV) and is comparable to kT around room temperature (0.026 eV), the formation of H–H with distances below 2.1 Å is limited to low temperatures and to a low number possibly undetected by diffraction methods. This is borne out by INS spectra on V–H which are strongly temperature dependent and reveal that the 55-meV peak does not exist at higher temperatures (33). This effect has been attributed to a transformation to different phases, with the 55-meV peak interpreted as in-plane modes of H occupying the octahedral site in β-V_2H. Our own first-principles calculations of the material with the Switendick criterion constraint do not reproduce this peak, supporting the notion that in V–H, hydrogen–hydrogen with distances below 2.1 Å occurs. A similar H–H pairing configuration has also been postulated in bcc tungsten, with a binding energy similar to that calculated for H–H in vanadium (32).

The relevance of the repulsive interactions goes beyond hydrogen storage: The minimum distance of hydrogen atoms in ordinary alloys never falls below 2.1 Å in metallic as well as covalent compounds (12). There has been great interest in converting molecular hydrogen into atomic metallic hydrogen with extraordinary properties such as superconductivity near room temperature (4). The required pressure to produce predicted structures with H–H distances slightly above 1 Å is close to 500 GPa (34). In contrast, other pressurized metal hydrides such as AlH_3 (35) have H–H distances from 2.54 Å at ambient pressure down to 1.54 Å at 110 GPa. In this sense, a close analog of atomic metallic hydrogen is LaH_{10}, which has comparable H–H linkages (5) and has been found to be a near room temperature superconductor at megabar pressures (7, 36). The evidence presented here for H–H distances of 1.64 Å in ZrV_2 is therefore of interest as it shows that this hydrogen configuration is thermodynamically possible at ambient pressure. The question of close H–H distances is also of interest from the standpoint of testing controversial claims for low-energy nuclear reactions in hydrogen-rich hydrides (37). The present study thus indicates the utility and importance of inelastic neutron scattering as a probe of the structures of hydrogen-rich materials with potentially novel properties.

Materials and Methods

Samples of ZrV_2 alloy (GfE Gesellschaft für Elektrometallurgie mbH) were crushed under a protective Ar atmosphere. Around 10 to 20 g of pristine ZrV_2 samples were wrapped in aluminum foil and then loaded into an aluminum high-pressure cell. The high-pressure cell was then mounted on a gas-handling sample stick. The samples were pumped to vacuum at room temperature and then cooled down to the measurement temperature. High-resolution INS spectra were measured at BL16-B (VISION), SNS, ORNL. After collecting the INS data for 12 h on the blank sample, the samples were taken out of the CCR for hydrogen dosing. For ZrV_2H_2, after holding at 400 °C for about 1 h, the sample was cooled again to base temperature (<15 K). For $ZrV_2H_{3.7}$, an annealing temperature of 100 °C was used (see *SI Appendix*, Fig. S3 for additional details). The amount of hydrogen gas adsorbed was used to calculate the hydrogen concentration in the alloy using the Sieverts method. INS data were collected for 12 h on the reacted sample for each temperature between 5 and 250 K for two hydrogen concentrations (ZrV_2H_2 and $ZrV_2H_{3.7}$). The specific compositions ZrV_2H_2 and $ZrV_2H_{3.7}$ were chosen, as they are particularly stable phases (24). The spectrum from a blank, corresponding to the total signal from the aluminum sample holder and the sample, was subtracted in all of the spectra shown. Preliminary INS spectra were also measured at the TOSCA and MARI beam lines at ISIS, Rutherford Appleton Laboratory.

Vibrational frequencies and vectors calculated using DFT methods were used to simulate the INS spectra with the oClimax software (19, 38, 39). The DFT calculations were performed with the plane-wave program VASP (40, 41) using projected augmented plane waves (PAW) (42, 43) to describe valence–core interactions and the generalized gradient approximation (GGA) with the Perdew–Burke–Ernzerhof (PBE) (44) parameterization of the exchange-correlation energy. A plane-wave cutoff of 500 eV was used for all energy minimization calculations at the gamma point. Using ^{T}H and ^{O}H to denote the regular hydrogens and the ones violating the Switendick criterion in $Zr_8V_{16}H_{32}$ atoms, the H atoms can be in any of the 32 ^{T}H and 96 ^{O}H available sites. We generated 100 random structures for different combinations of ^{T}H and ^{O}H with ^{O}H ranging from 1 to 32 (3,200 structures in total) and 1 for all 32 ^{T}H sites occupied (^{O}H=0) (Fig. 5).

The vibrational modes were calculated using CP2K, a PBE-type Goedecker–Teter–Hutter (GTH) pseudopotential combined with a double-valence polarized (DZVP) basis optimized for molecular calculations (DZVP-MOLOPT) (45–47). A 192-metal atom supercell of a primitive cell of cubic ZrV_2 with various concentrations of hydrogen atoms (128, 192, and 256 H atoms randomly occupying the ^{T}H and ^{O}H sites as defined in Fig. 1) was initially optimized using CP2K, followed by the normal mode calculations using the finite displacement methods with displacements of 0.01 Bohr. The SCF tolerance for the electronic structure calculations was $1 \cdot 10^{-7}$ eV and the force accuracy was within $1 \cdot 10^{-5}$ eV/Å. After convergence was reached, the force constants and the dynamical matrix were obtained from which the phonon frequencies and vibrational modes were calculated.

Principal experimental and computational data are contained in the main text and *SI Appendix*. All data files are available on request from the corresponding author.

ACKNOWLEDGMENTS. This research benefited from the use of the VISION beamline (IPTS-16527) at the Spallation Neutron Source, Oak Ridge National Laboratory (ORNL), which is supported by the Scientific User Facilities Division, Office of Basic Energy Sciences, US Department of Energy (DOE). This research used resources of the Oak Ridge Leadership Computing Facility at the ORNL, which is supported by the Office of Science of the DOE under Contract DE-AC05-00OR22725. oClimax is a part of the Integrated Computational Environment Modeling and Analysis of Neutron Data (ICEMAN) (LDRD 8237) project, funded by the Laboratory Directed Research and Development program at ORNL. This work was partly supported by the UZH-UFSP program LightChEC. We also acknowledge the financial support from the Swiss National Science Foundation (Grant 172662), the US NSF (DMR-1809783), and the US DOE/National Nuclear Security Administration (DE-NA0003858, CDAC). Financial support from NCBiR Project BIOSTRATEG2/297310/13/NCBR/2016 and CPU allocation at PL-Grid is also kindly acknowledged. Beam time at ISIS, Rutherford Appleton Laboratory is also greatly acknowledged. We thank Jon Taylor, Stewart Ross, Elsa Callini, and Andreas Züttel for help and support for measurements at the TOSCA and MARI beam lines, ISIS, Rutherford Appleton Laboratory, United Kingdom.

1. J. Alefeld, *Hydrogen in Metals I: Basic Properties*, J. Alefeld, G. Völkl, Eds. (Springer-Verlag, Berlin, Germany, 1978).
2. M. S. Dresselhaus, G. Dresselhaus, Intercalation compounds of graphite. *Adv. Phys.* **51**, 1–186 (2002).
3. M. Felderhoff, C. Weidenthaler, R. von Helmolt, U. Eberle, Hydrogen storage: The remaining scientific and technological challenges. *Phys. Chem. Chem. Phys.* **9**, 2643–2653 (2007).
4. N. W. Ashcroft, Hydrogen dominant metallic alloys: High temperature superconductors? *Phys. Rev. Lett.* **92**, 187002 (2004).
5. H. Liu, I. I. Naumov, R. Hoffmann, N. W. Ashcroft, R. J. Hemley, Potential high-T_c superconducting lanthanum and yttrium hydrides at high pressure. *Proc. Natl. Acad. Sci. U.S.A.* **117**, 6990–6995 (2017).
6. F. Peng *et al.*, Hydrogen clathrate structures in rare earth hydrides at high pressures: Possible route to room-temperature superconductivity. *Phys. Rev. Lett.* **119**, 107001 (2017).
7. M. Somayazulu *et al.*, Evidence for superconductivity above 260 K in lanthanum superhydride at megabar pressures. *Phys. Rev. Lett.* **122**, 027001 (2019).
8. Y. Fukai, *The Metal-Hydrogen System* (Springer-Verlag, Berlin, Germany, 2005).

9. K. Brownsberger *et al.*, X-ray diffraction, lattice structure, and equation of state of PdH_x and PdD_x to megabar pressures. *J. Phys. Chem. C* **121**, 27327–27331 (2017).
10. R. Lacher, A theoretical formula for the solubility of hydrogen in palladium. *Proc. R. Soc. A* **161**, 525–545 (1937).
11. E. Billeter, J. Terreni, A. Borgschulte, Hydride formation diminishes CO_2 reduction rate on palladium. *ChemPhysChem* **20**, 1398–1403 (2019).
12. A. C. Switendick, Band structure calculations for metal hydrogen systems. *Z. Phys. Chem.* **117**, 89–112 (1979).
13. B. K. Rao, P. Jena, Switendick criterion for stable hydrides. *Phys. Rev. B* **31**, 6726–6730 (1985).
14. V. A. Yartys *et al.*, Short hydrogen-hydrogen separations in novel intermetallic hydrides. *J. All. Comp.* **330–332**, 132–140 (2002).
15. A. N. Bogdanova, Neutron diffraction study of phase transitions in ZrV_2D_x ($4<x<5$). *Phys. Solid State* **48**, 1351–1355 (2006).
16. A. Pebler, E. A. Gulbransen, Equilibrium studies on the systems $ZrCr_2$-H_2, ZrV_2-H_2, and $ZrMo_2$-H_2 between 0° and 900°C. *Trans. Metall. Soc. AIME* **239**, 1593–1600 (1967).
17. J. J. Didisheim, K. Yvon, P. Fischer, D. Shaltiel, The deuterium site occupation in ZrV_2D_x as a function of the deuterium concentration. *J. Less Com. Met.* **73**, 355–362 (1980).
18. J. J. Didisheim *et al.*, The distribution of the deuterium atoms in the deuterated cubic laves-phase $ZrV_2D_{4.5}$. *Solid State Comm* **32**, 1087–1090 (1979).
19. P. C. H. Mitchell, S. F. Parker, A. J. Ramirez-Cuesta, J. Tomkinson, *Vibrational Spectroscopy with Neutrons with Applications in Chemistry, Biology, Materials Science and Catalysis*, J. L Finney, D. L Worcester, Eds. (World Scientific Publishing, Singapore, 2005).
20. P. Brüesch, *Phonons: Theory and Experiments II: Experiments and Interpretation of Experimental Results* (Springer, Heidelberg, Germany, 1986).
21. M. Rode *et al.*, Evidence for ionic bonding in $YH_{3-\delta}$. *Phys. Rev. Lett.* **87**, 235502 (2001).
22. A. I. Kolesnikov *et al.*, Lattice dynamics of high-pressure hydrides of the group VI - VIII transition metals. *Physica B* **316–317**, 158–161 (2002).
23. J. Dawidowski, F. J. Bermejo, J. R. Granada, Efficient procedure for the evaluation of multiple scattering and multiphonon corrections in inelastic neutron-scattering experiments. *Phys. Rev. B* **58**, 706–715 (1998).
24. R. Hempelmann, D. Richter, O. Hartmann, E. Karlsson, A. Wäppling, The positive muon in the intermetallic hydride ZrV_2H_x: A muon tracer study supplemented by differential thermoanalysis, neutron vibrational spectroscopy, and quasielastic neutron scattering. *J. Chem. Phys.* **90**, 1935–1949 (1980).
25. J. M. Rowe, J. J. Rush, H. G. Smith, M. Mostoller, H. E. Flotow, Lattice dynamics of a single crystal of $PdD_{0.63}$. *Phys. Rev. Lett.* **33**, 1297–1300 (1974).
26. J. J. Rush, H. E. Flotow, Vibration spectra of vanadium hydride in three crystal phases by inelastic neutron scattering. *J. Chem. Phys.* **48**, 3795–3804 (1968)
27. R. Gremaud *et al.*, Evidence for hydrogen transport in deuterated $libh_4$ from low-temperature Raman-scattering measurements and first-principles calculations. *Phys. Rev. B* **80**, 100301 (2009).
28. E. Mamontov, T. J. Udovic, O. Isnard, J. J. Rush, Neutron scattering study of hydrogen dynamics in $Pr_2Fe_{17}H_5$. *Phys. Rev. B* **70**, 1–5 (2004).
29. H. Smithson *et al.*, First-principles study of the stability and electronic structure of metal hydrides. *Phys. Rev. B* **66**, 144107 (2002).
30. S. K. Callear *et al.*, Understanding composition-property relationships in Ti-Cr-V-Mo alloys for optimisation of hydrogen storage in pressurised tanks. *Phys. Chem. Chem. Phys.* **16**, 16563–16572 (2014).
31. Y. Noda, T. Kajitani, M. Hirabyashi, S. Sato, X-ray structure determination of divanadium hydride, β_1-V_2H, and divanadium deuteride, β-V_2D. *Acta Cryst.* **C41**, 1566–1571 (1985).
32. C. Ouyang, Y. S. Lee, Hydrogen-induced interactions in vanadium from first-principles calculations. *Phys. Rev. B* **87**, 045111 (2011).
33. D. Klauder, V. Lottner, H. Scheuer, Investigation of the optic modes in $VH_{0.51}$ by neutron spectroscopy. *Solid State Com.* **32**, 617–620 (1979).
34. C. M. Pepin, G. Geneste, A. Dewaele, M. Mezouar, P. Loubeyre, Synthesis of FeH_5: A layered structure with atomic hydrogen slabs. *Science* **357**, 382–385 (2017).
35. I. Goncharenko *et al.*, Pressure-induced hydrogen-dominant metallic state in aluminum hydride. *Phys. Rev. Lett.* **100**, 045504 (2008).
36. A. P. Drozdov *et al.*, Superconductivity at 250 K in lanthanum hydride under high pressures. *Nature* **569**, 528–531 (2019).
37. C. P. Berlinguette *et al.*, Revisiting the cold case of cold fusion. *Nature* **570**, 45–51 (2019).
38. A. J. Ramirez-Cuesta, aCLIMAX 4.0.1, the new version of the software for analyzing and interpreting INS spectra. *Comput. Phys. Commun.* **157**, 226–238 (2004).
39. Y. Q. Cheng, L. L. Daemen, A. I. Kolesnikov, A. J. Ramirez-Cuesta, Simulation of inelastic neutron scattering spectra using OCLIMAX. *J. Chem. Theory Comput.* **15**, 1974–1982 (2019).
40. G. Kresse, J. Furthmm̈ller, Efficient iterative schemes for ab initio total-energy calculations using a plane-wave basis set. *Phys. Rev. B* **54**, 11169 (1996).
41. G. Kresse, J. Furthmüller, Efficiency of ab-initio total energy calculations for metals and semiconductors using a plane-wave basis set. *Comp. Mat. Sci.* **6**, 15–50 (1996).
42. P. E. Bloechl, Projector augmented-wave method. *Phys. Rev. B* **50**, 17953 (1994).
43. G. Kresse, D. Joubert, From ultrasoft pseudopotentials to the projector augmented-wave method. *Phys. Rev. B* **59**, 1758–1775 (1999).
44. J. P. Perdew, K. Burke, M. Ernzerhof, From ultrasoft pseudopotentials to the projector augmented-wave method. *Phys. Rev. Lett.* **77**, 3865–3868 (1996).
45. S. Goedecker, M. Teter, J. Hutter, Separable dual space Gaussian pseudo-potentials. *Phys. Rev. B* **54**, 1703–1710 (1996).
46. J. Hutter, M. Iannuzzi, F. Schiffmann, J. Vandevondele, CP2K: Atomistic simulations of condensed matter systems. *Wiley Interdiscip. Rev. Comput. Mol. Sci.* **4**, 15–25 (2014).
47. J. VandeVondele, J. Hutter, Gaussian basis sets for accurate calculations on molecular systems in gas and condensed phases. *J. Chem. Phys.* **127**:114105 (2007).